Functional hierarchy of oculomotor and visual motion subnetworks within the human cortical optokinetic system

Ria Maxine Ruehl[1,2], Felix Hoffstaedter[3,4], Andrew Reid[5], Simon Eickhoff[3,4], Peter zu Eulenburg[1,2]

1. *Department of Neurology, University Hospital, LudwigMaximilians-University Munich, 81377 Munich, Germany*
2. *German Center for Vertigo and Balance Disorders-IFB LMU, Ludwig-Maximilians-University Munich, 81377 Munich, Germany*
3. *Institute of Neuroscience and Medicine (INM-7), 52425 Juelich, Germany*
4. *Institute of Systems Neuroscience, Medical Faculty, Heinrich Heine University Düsseldorf, 40225 Duesseldorf, Germany*
5. *School of Psychology, University of Nottingham, Nottingham NG7 2RD, UK*

Abstract

Optokinetic look nystagmus (look OKN) is known to engage cortical visual motion and oculomotor hubs. Their functional network hierarchy, however, and the role of the cingulate eye field (CEF) and the dorsolateral prefrontal cortex (DLPFC) in particular have not been investigated. We used look OKN in fMRI to identify all cortical visual motion and oculomotor hubs involved. Using these activations as seed regions, we employed hierarchical clustering in two differing resting state conditions from a separate public data set. Robust activations in the CEF highlight its functional role in OKN and involvement in higher order oculomotor control. Deactivation patterns indicate a decreased modulatory involvement of the DLPFC. The hierarchical clustering revealed a changeable organization of the eye fields, hMT, V3A, and V6 depending on the resting state condition, segregating executive from higher order visual subnetworks. Overall, hierarchical clustering seems to allow for a robust delineation of physiological cortical networks.

Introduction

Voluntary and reflexive eye movements are controlled by complex neuronal pathways. On the supratentorial level, various hubs linked to the oculomotor system have been identified in primates, including the cortical eye fields [frontal- (FEF), supplementary- (SEF), parietal- (PEF), and cingulate- (CEF) eye fields], the dorsolateral prefrontal cortex (DLPFC), the basal ganglia, and areas hMT and V6 (Pierrot-Deseilligny et al. 2004; Krauzlis 2004; Konen et al. 2005; Shin and Sommer 2010).

However, the knowledge of the localization and function varies to a considerable extent between the individual hubs. Whereas the FEF have been studied extensively, less is known about the CEF, SEF, and PEF. Neural responses related to smooth pursuit eye movements, saccades, and horizontal optokinetic nystagmus (OKN) have been shown in the FEF and PEF, whereas the SEF seems to be mainly involved in motor programming of saccades, OKN, and only indirectly in higher level control of smooth pursuit (Dieterich et al. 2009; Bense et al.

2006; Krauzlis 2004). Regarding the functional role of CEF, functional imaging studies provided evidence for saccadic related activity, and increased latencies in several saccadic tasks were reported in lesion studies (Gaymard et al. 1998; Paus et al. 1993; Berman et al. 1999). The role of the DLPFC in oculomotor control seems to be the preparation of intentional saccades and inhibition of unwanted reflexive misdirected saccades (DeSouza et al. 2003; Ploner et al. 2005; Pierrot-Deseilligny et al. 2004). Subcortical circuits including the putamen, the globus pallidus (GP), and the thalamus modulate eye movements by means of feedback loops (Lynch and Tian 2006; Dieterich et al. 1998).

The optokinetic look nystagmus (look OKN) is a robust task to study ocular motor function. It is mainly cortically driven and has been shown to evoke stable responses in cortical oculomotor areas (Konen et al. 2005; Bense et al. 2006). Comprising a rhythmic train of slow tracking eye movements and contraversive resetting rapid eye movements, the OKN is fundamental to stabilize the retinal image during visual motion (Leigh and Zee 2006). Earlier studies have shown activations in different oculomotor hubs, but did not report activations in CEF or DLPFC (Dieterich et al. 2000, 2003b; Boileau et al. 2002; Galati et al. 1999; Bense et al. 2006; Konen et al. 2005; Bucher et al. 1997).

However, instead of aiming at localizing the individual ocular motor areas and defining their function, it might be more useful to focus on the oculomotor network as a system and its general hierarchical structure, especially with regard to the current knowledge of its dense functional interconnections. This approach might widen the understanding of how oculomotor and visual motion processing subnetworks interact and integrate information. Recent advances in sharing neuroimaging data offer the opportunity to characterize neural networks on large-scale data sets. A natural choice of method to delineate a functional network and decompose it into separate subunits is correlation-matrix-based hierarchical clustering in resting state data (Smith et al. 2015; Liu et al. 2012).

Here, we used hierarchical clustering to determine the functional hierarchy and the sub-clustering within the optokinetic network. The overarching idea was to examine whether resting state functional connectivity allows for a robust and replicable delineation of a previously established neural network.

First, we used a look-OKN task to delineate the cortical optokinetic network by means of fMRI. Here, we were particularly interested in responses of the CEF and the DLPFC. The main ocular motor seed regions were defined, including FEF, SEF, PEF, CEF, hMT, V6, V3A, GP, and DLPFC. To validate the network structure in a larger cohort and to assess the effect of the two most common resting state conditions on the ocular motor network's functional connectivity and the respective subgroups, we analyzed a publicly available data set, where fMRI was acquired at rest in "eyes open" and "eyes closed" conditions (Liu et al. 2013).

Materials and methods

fMRI experiment

Participants

Twenty healthy volunteers (10 female, mean age of 24.7 years) participated in the experiment after giving their informed written consent. The modified laterality quotient of handedness and footedness according to the 14-item inventory of the Edinburgh test (Chapman and Chapman 1987) was determined. With regard to potential interactions with the cortical vestibular network structure, all subjects had to be right-handed (Dieterich et al. 2003a). The participants were not allowed to take any medication regularly. Only subjects without a previous history of neurotological or neuroophthalmic disease or disorders of the central nervous system and

uncorrected vision (<3 dioptres) were included in the study. All volunteers underwent a diagnostic procedure prior to the fMRI experiment consisting of a clinical and electrophysiological examination of vertical and horizontal saccades, smooth pursuit, and optokinetic nystagmus by means of electronystagmography (ENG) to exclude pathological ocular motor function. This study was carried out in accordance with the Declaration of Helsinki (2013) and was approved by the local Ethics Committee. Subjects were paid for participation. The guidelines and principles for reporting fMRI studies laid down by Poldrack et al. (2008) were followed.

MRI protocol

Functional images were obtained with a clinical 3 T MRI scanner (Magnetom Verio, Siemens, Germany) and a 12-channel array head coil using echo-planar imaging (EPI) with a T2*-weighted gradient-echo sequence (TA 1.68 s, TE 30 ms, 31 continuous ascending axial slices covering the frontal, occipital, and parietal cortex with the main ocularmotor hubs, 3 mm isotropic voxels in plane, slice thickness 3 mm, field of view 192 mm2 , and flip angle 90°). The session consisted of 553 acquisition volumes. A high-resolution sagittal T1-weighted image (MPRAGE sequence, 176 slices, slice thickness 1 mm, image matrix 2562 , TR9.7 ms, and TE4 ms) was obtained for each subject.

Tasks and procedures

The optokinetic stimulus was presented via an adjustable mirror box reflecting the patterns onto a transparent custommade rear-projection screen attached to the head coil at a viewing distance of 19.5 cm (subject field of view 31.5° × 23.2°, target luminance 450 cd/m2 , blackstripes 50 cd/m2 , and luminance measured at the backside of the transparent projection screen). The scanner room was completely darkened. Smallfield-OKN was elicited using a square-wave grating pattern with a spatial frequency of 0.17 cyc/°, moving horizontally to the left or the right with a velocity of 30°/s. Images were presented with a temporal frequency of 5.2 Hz. The images were projected with a Christie LX-40 projector (Cypres, CA, USA) using a custom-made precision telescope lens system (Media Image GmbH, Zorneding, Germany). To reduce the perception of scanner noise, subjects wore earplugs in combination with covering head phones. The subject's forehead and chin were taped to the coil to minimize head movements.

The stimuli were presented in a randomized block design with a visual rest condition (eyes open), where the preceding stimulation pattern remained stationary. In this condition, subjects were advised to keep their gaze stable in the center of the screen. The duration of the visual rest condition varied between 8 and 11 blocks (duration from 13.44 to 18.48 s). The optokinetic stimulus to the left or right was shown for 9 blocks (duration of 15.12 s), respectively. Each stimulus was presented ten times (Fig. 1).

Prior to the experiment, subjects were trained to perform consistent look nystagmus outside the scanner. To ensure a correct and stable look-OKN performance and stable, straight gaze in the visual rest condition, the eye movements were monitored online from the scanner control room for all subjects with an infrared VOG unit (MEyeTrack-LR, SensoMotoric Instruments, SMI, Berlin/Boston; http://www.smi. com).

Data analysis of the task-based fMRI sessions

The statistical analysis was performed using SPM12 Version 6685 (Wellcome Department of Cognitive Neurology, London, UK) implemented in MatLab 2017a (MathWorks, Natick, MA).

Only subjects without morphological abnormalities or lesions in the anatomical images were included. To correct for subject movement, the images were realigned to the mean image of each scanning session. Stereotactical normalization was carried out to a resolution of 2×2×2 mm into the standard anatomical space as defined by the Montreal Neurological Institute (MNI) by means of the DARTEL algorithm onto the MNI template (http://nist.mni.mcgill.ca/?p=904) (Ashburner 2007). All stereotactic coordinates given in this paper refer to the MNI coordinate system. The normalized images were smoothed with a three-dimensional isotropic 6 mm Gaussian kernel during the DARTEL-based normalization process. To eliminate low-frequency noise and movement artifacts, a high-pass filter (128 s) was integrated into the design matrix. We estimated the effect of the different stimulus conditions on regional BOLD responses according to the general linear model (Friston et al. 1995b). Statistical parametric maps were generated on a voxel-byvoxel basis with a hemodynamic model of the stimulation periods present during the session (Friston et al. 1995a). For each stimulus condition, compared to the rest condition of each session, single subject t-contrasts were computed. To test for effects on a between-subject basis, the condition images were entered into a second-level statistical analysis. Paired t tests for the different directions of the OKN stimulus were performed using linear t-contrasts. Each stimulus condition was contrasted with the rest condition at the stage of the single-subject analysis. Results were considered significant at a voxel-level threshold of $p<0.05$ [false discovery rate (FDR) corrected]. Results were visualized using MRIcroGL by Chris Rhorden (https://www.nitrc.org/ frs/?group_id=889) after anatomical localisation with the anatomy toolbox (Eickhoff et al. 2005). Regions-of-interest (ROI) in both hemispheres for the subsequent connectivity analysis (FEF, SEF, CEF, PEF, V6, DLPFC, and GP) were extracted from the results. To segregate these ROIs clearly from the adjacent activation cluster and as we did not perform specific functional localizer to identify these areas, the ROIs for areas hMT and V3A were created using the SPM anatomy toolbox Version 2.2c (Eickhoff et al. 2007b).

Data and analysis of the resting-state fMRI

Resting-state fMRI data were analysed from the publicly available "Beijing: eyes open eyes closed sample" (Liu et al. 2013) including 48 subjects (24 female, mean age of 22.5 years) scanned in a 3 T TrioTim acquiring 240 EPI images in 6 min twice with eyes closed and eyes open (TR2 s, TE 30 ms, 33 continuous axial, 3.1 mm isotropic voxels in plane, slice thickness 3.5 mm, and field of view 200 mm2). To diminish the influence of physiological and movement artefacts on intrinsic resting-state fluctuations, FMRIB's ICA-based Xnoiseifier (FIX 1.06) was applied as implemented in FSL (5.0.9) (Salimi-Khorshidi et al. 2014). FIX decomposes the 4D imaging data into independent components and automatically classifies noise components using a large number of distinct spatial and temporal features via pattern classification relying on training datasets provided with FIX (Salimi-Khorshidi et al. 2014). Using the appropriate training data set (WhII_ Standard.RData) and settings recommended by Griffanti et al. (2014), variance uniquely related to the artefactual components was removed from each participant's raw data, which was shown to effectively remove noise from functional connectivity estimates without manual classification of noise components (Griffanti et al. 2016). The denoised EPI time series were further realigned using a two-pass procedure by which images were initially realigned to the first image and subsequently to the mean of the realigned images. Each participant's data were then spatially normalized to MNI space using the "unified segmentation" approach (Ashburner and Friston 2005). Finally, images were spatially smoothed by a 5-mm fullwidth at half-maximum Gaussian kernel and band-pass filtered preserving BOLD signal frequencies between 0.01 and 0.08 Hz. Each ROI was represented by the first eigenvariate of the respective voxels' time series and partial

correlations between all ROIs were computed using the FSLNets Toolbox (http://fsl.fmrib.ox.ac.uk/fsl/fslwiki/ FSLNets) to estimate pairwise functional connectivity (Marrelec et al. 2006). One group t tests were computed over Fisher's z-transformed correlation coefficients. The resulting t values were z-transformed and submitted to an agglomerative hierarchical cluster analysis using Ward's method as implemented in Matlab. Hierarchical clustering permits the heuristic identification of neurobiologically plausible and functionally interpretable subclusters within the network for ocular motor control.

In comparison with other functional connectivity data-driven methods, the correlation-matrix-based hierarchical clustering method is able to detect even weak functional connectivity patterns with a high sensitivity, also in a single data set (Liu et al. 2012). Under the resting state (RS) condition in the absence of any task, spontaneous neuronal activity is present as means of low-frequency (<0.08 Hz) fluctuations in the BOLD signal (Biswal et al. 1995). Correlations of these responses across different areas can be used to identify coherent activity patterns and to characterize functional networks (Fox and Raichle 2007). Applying clustering algorithms on resting state functional connectivity between previously defined brain regions allows for a functional parcellation of the underlying network, based on the distance matrix of node-to-node interactions (Fox and Raichle 2007). The resulting set of nested clusters can then be visualized as a dendrogram, which documents the sequences of merges or splits.

Results

Activations during OKN stimulation

Horizontal OKN stimulation led to robust activations in the ocular motor network, including the FEF, SEF, CEF, PEF, the thalamus, putamen and GP, as well as primary visual and visual motion areas, including hMT+, area V6 and V3A in both hemispheres (see Table 1; Fig. 2). Direction-dependent activations were found in the PEF and in area V3A ipsilateral to the stimulation direction, whereas V6 showed stronger contralateral activations (Fig. 2a).

Deactivations

Optokinetic stimulation led to deactivations in the rolandic operculum (including areas OP3, OP4) and the posterior insula (including Ig2) in both hemispheres (Fig. 2b). Further deactivations were clustered in the precentral gyrus, the superior, middle and posterior frontal gyrus, and the anterior and middle cingulate cortex (Fig. 2b). Larger deactivation cluster and higher t values were found in the dorsolateral prefrontal cortex (DLPFC) of the right hemisphere. The DLPFC also showed a direction-dependent deactivation with higher t values and larger cluster sizes contralateral to the stimulus direction.

Hierarchical clustering

Supervised hierarchical clustering of functional connectivity between areas involved in optokinetic look nystagmus showed differential results for the eyes open and the eyes closed conditions at rest. For both conditions, only DLPFC and GP formed a consistent cluster, while the cortical eye fields and higher visual areas showed a condition specific pattern. Without visual input, V6, V3A, hMT, and PEF formed a posterior subcluster opposed to the remaining cortical eye fields SEF, FEF, and CEF as an anterior subcluster surrounding DLPFC and GP (Fig. 3). Constant visual input in the resting state with eyes open revealed a close association

of V3A and hMT with DLPFC and GP, which altogether were associated with FEF and PEF, leaving CEF, SEF, and V6 as a separate subcluster (Fig. 3). A switch in order and grouping of the subclusters was observed for all seeds, with the exception of DLPFC and GP (Fig. 4): SEF switched from a subcluster with FEF in the eyes closed condition to a subcluster with CEF in the eyes open condition. CEF formed a separate subcluster in the eyes closed condition. FEF on the other hand switched to a subcluster with PEF in the eyes open condition. PEF was grouped in the eyes closed condition with hMT. In the eyes open condition, hMT formed a subcluster with area V3A, which in the eyes closed condition was grouped with V6, while V6 was clustered separately in the eyes open condition.

Discussion

Horizontal look OKN gave robust activations in the main cortical oculormotor hubs. For the first time, we show an involvement of all cortical eye fields, including CEF, in the optokinetic nystagmus, as well as direction-dependent responses. The deactivation pattern hints at a sensory inhibition during OKN. Our results indicate a permanent involvement of the CEF in the oculomotor network and further strengthen the hypothesis of its rather supervisory control function, together with SEF. Hierarchical clustering revealed a different functional subgrouping of the cortical eye fields, hMT, V3A, and V6 in the optokinetic network, depending on the resting state condition, whereas DLPFC and GP formed a constant subcluster in both tasks. Executive oculomotor (FEF, PEF) and afferent intermediate-level visual motion processing regions (V3A, hMT) build a functional subgroup separate from higher order visual and oculomotor regions (CEF, SEF, V6) in the eyes open condition. With eyes closed, mainly oculomotor-related regions (SEF, FEF, and CEF) were separated from visual stream-related regions (PEF, hMT, V3A, and V6), yielding an expected differentiation between systems for bottom–up visual and more top–down oculomotor systems without visual input. The switch of subclustering might also be explained by a differential involvement of the image-stabilizing optokinetic system in the eyes open and eyes closed condition.

Deactivation pattern during OKN

Deactivation patterns revealed bilateral signal decreases of DLPFC (Fig. 2b). Recently, a functional division of the DLPFC was suggested, which a posterior subregion involved in action execution and working memory (Cieslik et al. 2013). The deactivation of this subregion in our experiment might be explained by the repetitive task character with fast automatic eye movements in the same direction. This implicates potential hinderance of modulatory involvement of the DLPFC. Furthermore, our data show deactivations in the parietal operculum, including area OP3 and OP4, but not in vestibular core region OP2. Cytoarchitectonic areas OP3 and OP4 represent primate areas ventral somatosensory area (VS) and parietal ventral area (PV) (Eickhoff et al. 2006, 2007a). Both areas contain a face representation and show robust bilateral responses to unilateral sensory stimulation (Eickhoff et al. 2008). Our results might reflect a suppression of sensory input from the eye lid and orbita during repetitive voluntary eye movements. The parallel deactivations in the blinking-associated middle cingulate gyrus further substantiate this hypothesis (Hanakawa et al. 2008).

Functional subdivisions of the OKN networks

FEF and PEF

Our analysis revealed a subclustering of FEF and PEF in the eyes open condition only (Fig. 3). The FEF plays a crucial role in the generation of saccades, pursuit eye movements, OKN, and the allocation of spatial attention (Everling 2007; Blanke et al. 2000; Pierrot-Deseilligny et al. 2004; Dieterich et al. 2003b). PEF, on the other hand, is involved in the control of reflexive visually guided saccades and visual attention (Brotchie et al. 2003; Buchel et al. 1998).

The subclustering of both regions highlights their functional proximity within the optokinetic network and corresponds well to studies in nonhuman primates, showing dense reciprocal connections (Schall et al. 1993; Tian and Lynch 1996). In the eyes-closed condition, we found a switch of subclusters, with PEF grouped together with hMT, V3A, and V6 (Fig. 4).

Animal literature provides evidence that these areas form part of the dorsal visual stream (Gilaie-Dotan 2016). Contrasting with human PEF, the corresponding area LIP has been studied extensively. It occupies a high position in the dorsal visual stream and responds primarily to saccades in relation with smooth pursuit (Felleman and Van Essen 1991; Andersen et al. 1990). A recent study gave evidence for two subdivisions of LIP, with the ventral part related to saccades and the dorsal part associated with visual processing (Chen et al. 2016). Our data suggest a similar functional range of human PEF pointing at a preponderance of the executive oculomotor function in the eyes-open condition. Differential functional roles of PEF and FEF in humans have to be clarified yet, in particular with respect to a further functional subdivision. Therefore, when interpreting our results, it should be considered that the ROIs in our study were defined by an OKN task and will not include functional subdivisions. In addition, with regard to the hierarchical clustering results, a major limiting factor is the resolution of the functional images, which determines the number of levels in the hierarchical clustering analysis.

CEF, SEF, and FEF

The CEF showed robust bilateral activations during horizontal OKN, and its functional importance in the optokinetic and oculomotor network is further substantiated by the results of the hierarchical clustering analysis (Figs. 2,3,4). To date, only few investigated its role in oculomotor control, showing in a decreased gain of memory-guided saccades and increased latency in an antisaccade task after lesions in this region (Gaymard et al. 1998).

In line with our results, CEF and SEF have been shown to share some functional properties. SEF is involved in antisaccades and memory-guided saccades (Parton et al. 2007), and similar to CEF, a supervisory function for oculomotor control has been suggested (Stuphorn and Schall 2002; Huerta and Kaas 1990). The fact that in the eyes open condition, both CEF and SEF build a separate subcluster from the rather executive operating regions FEF and PEF could be further interpreted within the course of their predominant role in higher oculomotor control.

DLPFC and GP

The DLPFC and GP showed a consistent subclustering, independent of the resting state condition (Figs. 3,4). Both brain regions are supposed to modulate eye movements by inhibitory influences, exerting a predominantly integrative and coordinative function (Alexander et al. 1986; Pierrot-Deseilligny et al. 2004). The GP as part of the basal ganglia has been recently shown to be involved in saccades, smooth pursuit and also in OKN (Bucher et al.

1997; Yoshida and Tanaka 2009; Shin and Sommer 2010). In contrast to other parts of the basal ganglia, its role in oculomotor function and its connections to oculomotor regions are less well understood. A direct cortical pathway via the putamen to the globus pallidus interna and an indirect pathway via the globus pallidus externa has been established in animal literature (Handel and Glimcher 2000; Shin and Sommer 2010). In addition, the DLPFC has been shown to play a vital role in memory guided saccades and saccade inhibition (DeSouza et al. 2003; Pierrot-Deseilligny et al. 2003). This close functional relationship of between the DLPFC and GP is further consolidated by our findings, while their structural connectivity pathways could be the focus of future studies.

hMT, V3A, and V6

In the eyes closed condition, V3A and V6 formed a subcluster and were grouped with area PEF and hMT (Fig. 3). Our results thus extend data in the macaque, indicating that areas V3A and V6 rank hierarchically on the same level as MT/V5 (Shipp et al. 1998). The subgrouping of area V6 and V3A is strongly supported by animal literature, showing dense reciprocal interconnections between V3A and V6 (Zeki 1978; Galletti and Battaglini 1989).

The switch of subclusters in the eyes open condition with the clustering of hMT and V3A (Fig. 4) is in line with their intermediate position in the visual processing hierarchical structure and their crucial role in visual motion, speed, and contrast perception (Tootell et al. 1997; McKeefry et al. 2008). Interestingly, V6 appears to take a unique position, forming a single cluster in the same subgroups as CEF and SEF (Fig. 4). In comparison with other visual motion areas, the strong sensitivity to depth gradients seems to be an outstanding feature of V6, suggesting a key role in navigation in dense environments and egomotion (Cardin and Smith 2011). V6 is responding especially to peripheral stimulation of the visual field, distinct from V3A and hMT, which are involved in the analysis of motion signals particularly in the central part of the visual field (Pitzalis et al. 2012, 2015; Press et al. 2001). Reciprocal connections to visual areas like MST and VIP further substantiate this presumed functional role (Galletti et al. 2001; Shipp et al. 1998). Our results further underline the outstanding features of V6. Its subgrouping with areas CEF and SEF might indicate a stronger functional role in goal directed behavior, as well as its central function as a hub conveying self-motion-related information on objects in depth to other higher visual areas, thereby enabling coordinated eye and arm movements (Pitzalis et al. 2015).

Conclusion

The fMRI experiment revealed a strong involvement of all cortical eye fields, visual motion-processing areas, and the basal ganglia in optokinetic control. Our results underpin the essential role and importance of the CEF in optokinetic look nystagmus and within the oculomotor network in general, hinting at a functional characterization of CEF as a higher order oculomotor region together with SEF, and separate from the frontal and parietal eye fields. Deactivations in cytoarchitectonic area OP3, OP4 and blinking movement related midcingulate cortex suggest a suppression of sensory input from the eyes and the orbita during OKN. Signal decreases in right DLPFC hint at a diminished modulatory input during the repetitive eye movements of horizontal OKN.

Hierarchical clustering analysis showed a differential organization of subclusters as a function of the respective resting state condition. In the eyes open condition, hierarchical clustering separated higher order visual and oculomotor regions (CEF, SEF, V6) from rather executive oculomotor regions (FEF, PEF) and afferent intermediate level visual motion-

processing regions (V3A, hMT). Without visual input, a subgrouping of regions which form part of the visual stream (PEF, hMT, V3A, V6) could be delineated from predominantly oculomotor-related regions (SEF, FEF, CEF). This switch of subclusters might be explained by a stronger involvement of the optokinetic system in the eyes open condition, in which stabilization of the retinal image is vital, in contrast to the eyes closed condition. Furthermore, in the subcluster, structure hints at the wide range of functional properties of these brain structures as shown by various functional studies. Only DLPFC and GP, mainly associated with inhibitory functions, formed a constant cluster in both conditions, consistent with their proposed roles as supervisory gatekeepers for cortical ocularmotor control. Finally, our results substantiate the feasibility of hierarchical clustering as a method to delineate the underlying network structure in a physiological system.

References

Alexander GE, DeLong MR, Strick PL (1986) Parallel organization of functionally segregated circuits linking basal ganglia and cortex. Annu Rev Neurosci 9:357–381. https://doi.org/10.1146/annur ev.ne.09.030186.002041

Andersen RA, Bracewell RM, Barash S, Gnadt JW, Fogassi L (1990) Eye position effects on visual, memory, and saccade-related activity in areas LIP and 7a of macaque. J Neurosci 10(4):1176–1196

Ashburner J (2007) A fast diffeomorphic image registration algorithm. NeuroImage 38(1):95–113. https://doi.org/10.1016/j.neuroimage .2007.07.007

Bense S, Janusch B, Schlindwein P, Bauermann T, Vucurevic G, Brandt T, Stoeter P, Dieterich M (2006) Direction-dependent visual cortex activation during horizontal optokinetic stimulation (fMRI study). Hum Brain Mapp 27(4):296–305. https://doi.org/10.1002/ hbm.20185

Berman RA, Colby CL, Genovese CR, Voyvodic JT, Luna B, Thulborn KR, Sweeney JA (1999) Cortical networks subserving pursuit and saccadic eye movements in humans: an FMRI study. Hum Brain Mapp 8(4):209–225

Biswal B, Yetkin FZ, Haughton VM, Hyde JS (1995) Functional connectivity in the motor cortex of resting human brain using echoplanar MRI. Magn Reson Med 34(4):537–541

Blanke O, Spinelli L, Thut G, Michel CM, Perrig S, Landis T, Seeck M (2000) Location of the human frontal eye field as defined by electrical cortical stimulation: anatomical, functional and electrophysiological characteristics. Neuroreport 11(9):1907–1913

Boileau I, Beauregar M, Beuter A, Breault C, Lecours AR (2002) Optokinetic stimulation and the egocentred midsagittal plane: an fMRI study. Neuroreport 13(1):61–65

Brotchie PR, Lee MB, Chen DY, Lourensz M, Jackson G, Bradley WG Jr (2003) Head position modulates activity in the human parietal eye fields. NeuroImage 18(1):178–184

Buchel C, Josephs O, Rees G, Turner R, Frith CD, Friston KJ (1998) The functional anatomy of attention to visual motion. A functional MRI study. Brain J Neurol 121(Pt 7):1281–1294

Bucher SF, Dieterich M, Seelos KC, Brandt T (1997) Sensorimotor cerebral activation during optokinetic nystagmus. A functional MRI study. Neurology 49(5):1370–1377

Cardin V, Smith AT (2011) Sensitivity of human visual cortical area V6 to stereoscopic depth gradients associated with self-motion. J Neurophysiol 106(3):1240

Chapman LJ, Chapman JP (1987) The measurement of handedness. Brain Cogn 6(2):175–183

Chen M, Li B, Guang J, Wei L, Wu S, Liu Y, Zhang M (2016) Two subdivisions of macaque LIP process visual-oculomotor information differently. Proc Natl Acad Sci USA 113(41):E6263– E6270. https://doi.org/10.1073/pnas.1605879113

Cieslik EC, Zilles K, Caspers S, Roski C, Kellermann TS, Jakobs O, Langner R, Laird AR, Fox PT, Eickhoff SB (2013) Is there "one" DLPFC in cognitive action control? Evidence for heterogeneity from co-activation-based parcellation. Cereb Cortex 23(11):2677–2689. https://doi.org/10.1093/cercor/bhs256

DeSouza JF, Menon RS, Everling S (2003) Preparatory set associated with pro-saccades and anti-saccades in humans investigated with event-related FMRI. J Neurophysiol 89(2):1016–1023. https://doi.org/10.1152/jn.00562.2002

Dieterich M, Bucher SF, Seelos KC, Brandt T (1998) Horizontal or vertical optokinetic stimulation activates visual motionsensitive, ocular motor and vestibular cortex areas with right hemispheric dominance. An fMRI study. Brain J Neurol 121(Pt 8):1479–1495

Dieterich M, Bucher SF, Seelos KC, Brandt T (2000) Cerebellar activation during optokinetic stimulation and saccades. Neurology 54(1):148–155

Dieterich M, Bense S, Lutz S, Drzezga A, Stephan T, Bartenstein P, Brandt T (2003a) Dominance for vestibular cortical function in the non-dominant hemisphere. Cereb Cortex 13(9):994–1007

Dieterich M, Bense S, Stephan T, Yousry TA, Brandt T (2003b) fMRI signal increases and decreases in cortical areas during small-field optokinetic stimulation and central fixation. Exp Brain Res 148(1):117–127. https://doi.org/10.1007/s0022 1-002-1267-6

Dieterich M, Muller-Schunk S, Stephan T, Bense S, Seelos K, Yousry TA (2009) Functional magnetic resonance imaging activations of cortical eye fields during saccades, smooth pursuit, and optokinetic nystagmus. Ann N Y Acad Sci 1164:282–292. https://doi.org/10.1111/j.1749-6632.2008.03718.x

Eickhoff SB, Stephan KE, Mohlberg H, Grefkes C, Fink GR, Amunts K, Zilles K (2005) A new SPM toolbox for combining probabilistic cytoarchitectonic maps and functional imaging data. NeuroImage 25(4):1325–1335. https://doi.org/10.1016/j.neuroimage .2004.12.034

Eickhoff SB, Schleicher A, Zilles K, Amunts K (2006) The human parietal operculum. I. Cytoarchitectonic mapping of subdivisions. Cereb Cortex 16(2):254–267. https://doi.org/10.1093/cercor/bhi10 5

Eickhoff SB, Grefkes C, Zilles K, Fink GR (2007a) The somatotopic organization of cytoarchitectonic areas on the human parietal operculum. Cereb Cortex 17(8):1800–1811. https://doi. org/10.1093/cercor/bhl090

Eickhoff SB, Paus T, Caspers S, Grosbras MH, Evans AC, Zilles K, Amunts K (2007b) Assignment of functional activations to probabilistic cytoarchitectonic areas revisited. NeuroImage 36(3):511– 521. https://doi.org/10.1016/j.neuroimage.2007.03.060

Eickhoff SB, Grefkes C, Fink GR, Zilles K (2008) Functional lateralization of face, hand, and trunk representation in anatomically defined human somatosensory areas. Cereb Cortex 18(12):2820– 2830. https://doi.org/10.1093/cercor/bhn039

Everling S (2007) Where do I look? From attention to action in the frontal eye field. Neuron 56(3):417–419. https://doi.org/10.1016/j. neuron.2007.10.026

Felleman DJ, Van Essen DC (1991) Distributed hierarchical processing in the primate cerebral cortex. Cereb Cortex 1(1):1–47

Fox MD, Raichle ME (2007) Spontaneous fluctuations in brain activity observed with functional magnetic resonance imaging. Nat Rev Neurosci 8(9):700–711. https://doi.org/10.1038/nrn2201

Friston KJ, Frith C, Turner R, Frackowiak RSJ (1995a) Characterizing evoked hemodynamics with fMRI. NeuroImage 2:157–165

Friston KJ, Holmes AP, Worsley KJ, Poline JB, Frith C, Frackowiak RSJ (1995b) Statistical parametric maps in functional imaging: a general linear approach. Hum Brain Mapp 2:189–210

Galati G, Pappata S, Pantano P, Lenzi GL, Samson Y, Pizzamiglio L (1999) Cortical control of optokinetic nystagmus in humans: a positron emission tomography study. Exp Brain Res 126(2):149–159

Galletti C, Battaglini PP (1989) Gaze-dependent visual neurons in area V3A of monkey prestriate cortex. J Neurosci 9(4):1112

Galletti C, Gamberini M, Kutz DF, Fattori P, Luppino G, Matelli M (2001) The cortical connections of area V6: an occipitoparietal network processing visual information. Eur J Neurosci 13(8):1572–1588

Gaymard B, Rivaud S, Cassarini JF, Dubard T, Rancurel G, Agid Y, Pierrot-Deseilligny C (1998) Effects of anterior cingulate cortex lesions on ocular saccades in humans. Exp Brain Res 120(2):173–183

Gilaie-Dotan S (2016) Visual motion serves but is not under the purview of the dorsal pathway. Neuropsychologia 89:378–392. https ://doi.org/10.1016/j.neuropsychologia.2016.07.018

Griffanti L, Salimi-Khorshidi G, Beckmann CF, Auerbach EJ, Douaud G, Sexton CE, Zsoldos E, Ebmeier KP, Filippini N, Mackay CE, Moeller S, Xu J, Yacoub E, Baselli G, Ugurbil K, Miller KL, Smith SM (2014) ICA-based artefact removal and accelerated

fMRI acquisition for improved resting state network imaging. NeuroImage 95:232–247. https://doi.org/10.1016/j.neuroimage .2014.03.034

Griffanti L, Rolinski M, Szewczyk-Krolikowski K, Menke RA, Filippini N, Zamboni G, Jenkinson M, Hu MTM, Mackay CE (2016) Challenges in the reproducibility of clinical studies with resting state fMRI: an example in early Parkinson's disease. NeuroImage 124(Pt A):704–713. https://doi.org/10.1016/j.neuroimage .2015.09.021

Hanakawa T, Dimyan MA, Hallett M (2008) The representation of blinking movement in cingulate motor areas: a functional magnetic resonance imaging study. Cereb Cortex 18(4):930–937. https ://doi.org/10.1093/cercor/bhm129

Handel A, Glimcher PW (2000) Contextual modulation of substantia nigra pars reticulata neurons. J Neurophysiol 83(5):3042–3048

Huerta MF, Kaas JH (1990) Supplementary eye field as defined by intracortical microstimulation: connections in macaques. J Comp Neurol 293(2):299–330

Konen CS, Kleiser R, Seitz RJ, Bremmer F (2005) An fMRI study of optokinetic nystagmus and smooth-pursuit eye movements in humans. Exp Brain Res 165(2):203–216. https://doi.org/10.1007/ s00221-005-2289-7

Krauzlis RJ (2004) Recasting the smooth pursuit eye movement system. J Neurophysiol 91(2):591

Leigh RJ, Zee DS (2006) The neurology of eye movements, 4th edn. Oxford University Press, Oxford

Liu X, Zhu XH, Qiu P, Chen W (2012) A correlation-matrix-based hierarchical clustering method for functional connectivity analysis. J Neurosci Methods 211(1):94–102. https://doi.org/10.1016/j. jneumeth.2012.08.016

Liu D, Dong Z, Zuo X, Wang J, Zang Y (2013) Eyes-open/eyes-closed dataset sharing for reproducibility evaluation of resting state fMRI data analysis methods. Neuroinformatics 11(4):469–476. https:// doi.org/10.1007/s12021-013-9187-0

Lynch JC, Tian JR (2006) Cortico-cortical networks and cortico-subcortical loops for the higher control of eye movements. Prog Brain Res 151:461–501. https://doi.org/10.1016/s0079-6123(05)51015 -x

Marrelec G, Krainik A, Duffau H, Pelegrini-Issac M, Lehericy S, Doyon J, Benali H (2006) Partial correlation for functional brain interactivity investigation in functional MRI. NeuroImage 32(1):228–237. https://doi.org/10.1016/j.neuroimage.2005.12.057

McKeefry DJ, Burton MP, Vakrou C, Barrett BT, Morland AB (2008) Induced deficits in speed perception by transcranial magnetic stimulation of human cortical areas V5/MT + and V3A. J Neurosci 28(27):6848–6857. https://doi.org/10.1523/jneur osci.1287-08.2008

Parton A, Nachev P, Hodgson TL, Mort D, Thomas D, Ordidge R, Morgan PS, Jackson S, Rees G, Husain M (2007) Role of the human supplementary eye field in the control of saccadic eye movements. Neuropsychologia 45(5-4):997–1008. https://doi.org/10.1016/j. neuropsychologia.2006.09.007

Paus T, Petrides M, Evans AC, Meyer E (1993) Role of the human anterior cingulate cortex in the control of oculomotor, manual, and speech responses: a positron emission tomography study. J Neurophysiol 70(2):453–469

Pierrot-Deseilligny C, Muri RM, Ploner CJ, Gaymard B, Demeret S, Rivaud-Pechoux S (2003) Decisional role of the dorsolateral prefrontal cortex in ocular motor behaviour. Brain J Neurol 126(Pt 6):1460–1473

Pierrot-Deseilligny C, Milea D, Muri RM (2004) Eye movement control by the cerebral cortex. Curr Opin Neurol 17(1):17–25

Pitzalis S, Fattori P, Galletti C (2012) The functional role of the medial motion area V6. Front Behav Neurosci 6:91. https://doi. org/10.3389/fnbeh.2012.00091

Pitzalis S, Fattori P, Galletti C (2015) The human cortical areas V6 and V6A. Vis Neurosci 32:E007. https://doi.org/10.1017/s0952 523815000048

Ploner CJ, Gaymard BM, Rivaud-Pechoux S, Pierrot-Deseilligny C (2005) The prefrontal substrate of reflexive saccade inhibition in humans. Biol Psychiatry 57(10):1159–1165. https://doi. org/10.1016/j.biopsych.2005.02.017

Poldrack RA, Fletcher PC, Henson RN, Worsley KJ, Brett M, Nichols TE (2008) Guidelines for reporting an fMRI study. NeuroImage 40(2):409–414. https://doi.org/10.1016/j.neuroimage.2007.11.048

Press WA, Brewer AA, Dougherty RF, Wade AR, Wandell BA (2001) Visual areas and spatial summation in human visual cortex. Vis Res 41(10–11):1321–1332

Salimi-Khorshidi G, Douaud G, Beckmann CF, Glasser MF, Griffanti L, Smith SM (2014) Automatic denoising of functional MRI data: combining independent component analysis and hierarchical fusion of classifiers. NeuroImage 90:449–468. https://doi. org/10.1016/j.neuroimage.2013.11.046

Schall JD, Morel A, Kaas JH (1993) Topography of supplementary eye field afferents to frontal eye field in macaque: implications for mapping between saccade coordinate systems. Vis Neurosci 10(2):385–393

Shin S, Sommer MA (2010) Activity of neurons in monkey globus pallidus during oculomotor behavior compared with that in substantia nigra pars reticulata. J Neurophysiol 103(4):1874–1887. https:// doi.org/10.1152/jn.00101.2009

Shipp S, Blanton M, Zeki S (1998) A visuo-somatomotor pathway through superior parietal cortex in the macaque monkey: cortical connections of areas V6 and V6A. Eur J Neurosci 10(10):3171–3193

Smith SM, Nichols TE, Vidaurre D, Winkler AM, Behrens TE, Glasser MF, Ugurbil K, Barch DM, Van Essen DC, Miller KL (2015) A positive-negative mode of population covariation links brain connectivity, demographics and behavior. Nat Neurosci 18(11):1565– 1567. https://doi.org/10.1038/nn.4125

Stuphorn V, Schall JD (2002) Neuronal control and monitoring of initiation of movements. Muscle Nerve 26(3):326–339. https://doi. org/10.1002/mus.10158

Tian JR, Lynch JC (1996) Corticocortical input to the smooth and saccadic eye movement subregions of the frontal eye field in Cebus monkeys. J Neurophysiol 76(4):2754–2771

Tootell RB, Mendola JD, Hadjikhani NK, Ledden PJ, Liu AK, Reppas JB, Sereno MI, Dale AM (1997) Functional analysis of V3A and related areas in human visual cortex. J Neurosci 17(18):7060–7078

Yoshida A, Tanaka M (2009) Neuronal activity in the primate globus pallidus during smooth pursuit eye movements. Neuroreport 20(2):121–125. https://doi.org/10.1097/WNR.0b013e32831af055

Zeki SM (1978) Uniformity and diversity of structure and function in rhesus monkey prestriate visual cortex. J Physiol 277:273–290

Figures

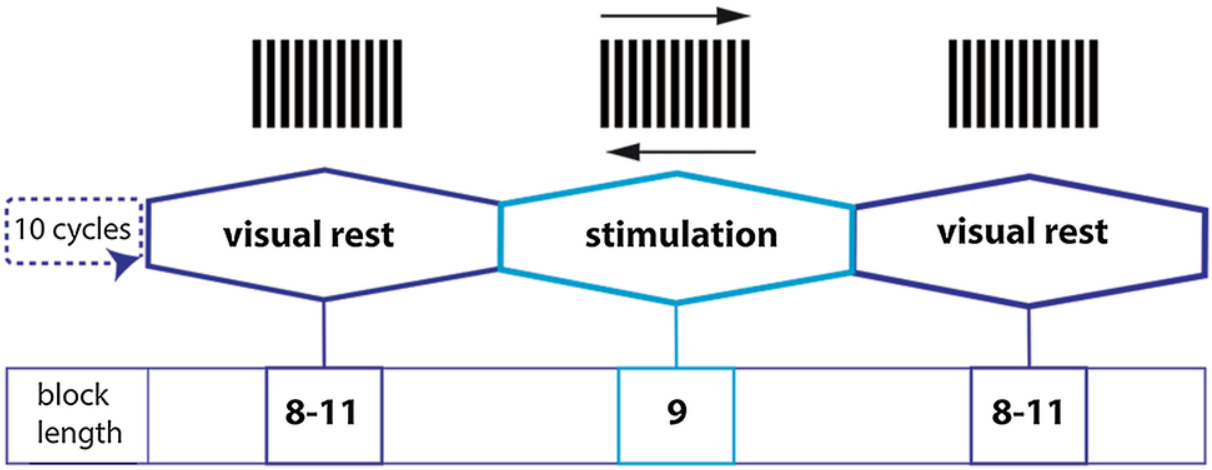

Figure 1. Schematic draft of the experimental design. A randomized block design with a visual rest condition (eyes open) varying in duration (visual rest condition 8–11 blocks and stimulus condition 9 blocks) was used. The stimulus consisted of a square-wave grating pattern, moving horizontally with a velocity of 30°/s to the left or right. Each stimulus was presented ten times. During the visual rest condition, the preceding stimulation pattern remained stationary.

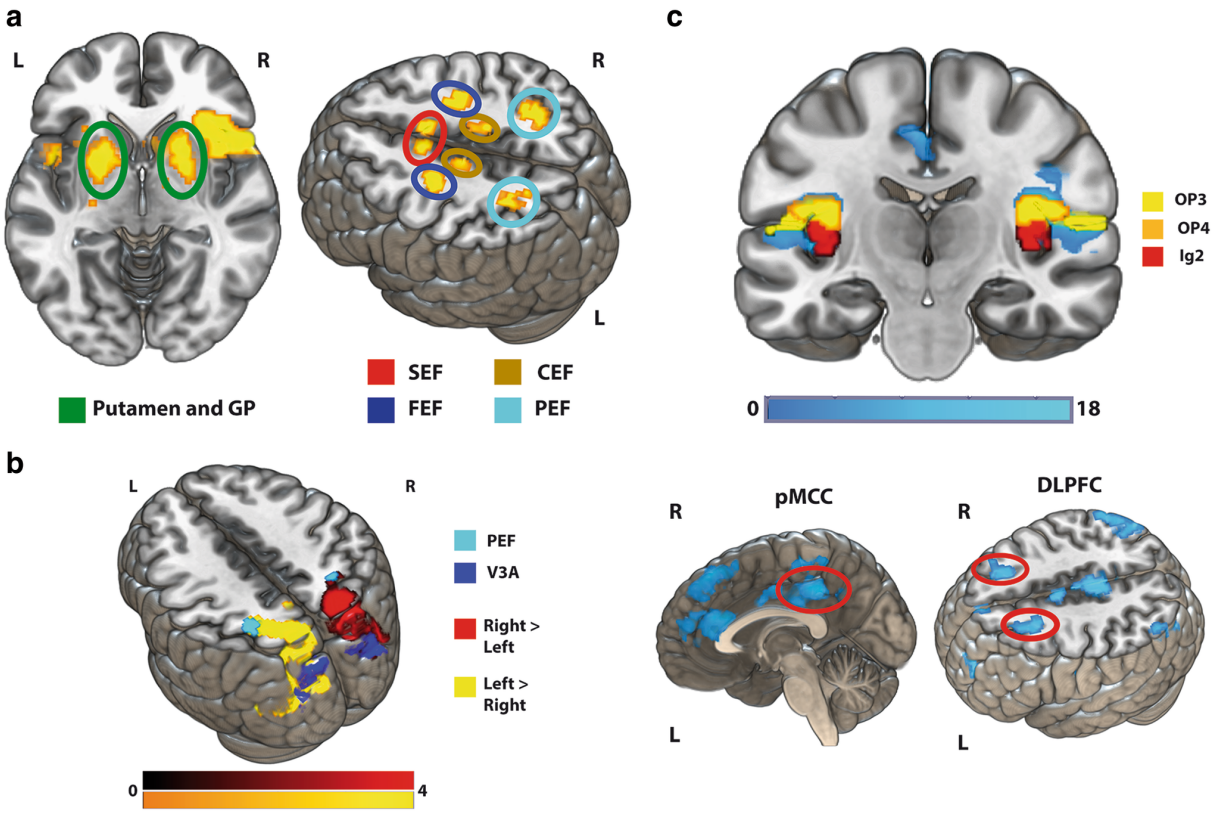

Figure 2. Activation and deactivation patterns during horizontal look OKN. **(a)** Horizontal OKN led to robust activations in all cortical eye fields (right top image, SEF in red, FEF in blue, CEF in beige, and PEF light blue) and in in the putamen and GP (left top image, green). The scales depict z scores. **(b)** Direction-dependent activations (bottom image, right > left in red, and left > right in yellow) were found in PEF (light blue), V3A (dark blue), and V6 (not shown). The scales depict z scores. **(c)** Deactivations in the parietal operculum (blue, top image) during OKN, with global maxima in cytoarchitectonic area OP3 (yellow overlay), OP4 (orange overlay), and Ig2 (red overlay) indicate a multisensory inhibition during OKN, probably including the somatosensory representation of the eye and orbita. Signal decreases in the blink-movement-related anterior, and posterior midcingulate cortex (pMCC, left bottom image) can be interpreted in the same context. The deactivations of the DLPFC (right bottom image) hint at a diminished modulatory involvement during the performance of repetitive eye movements. All scales depict z scores.

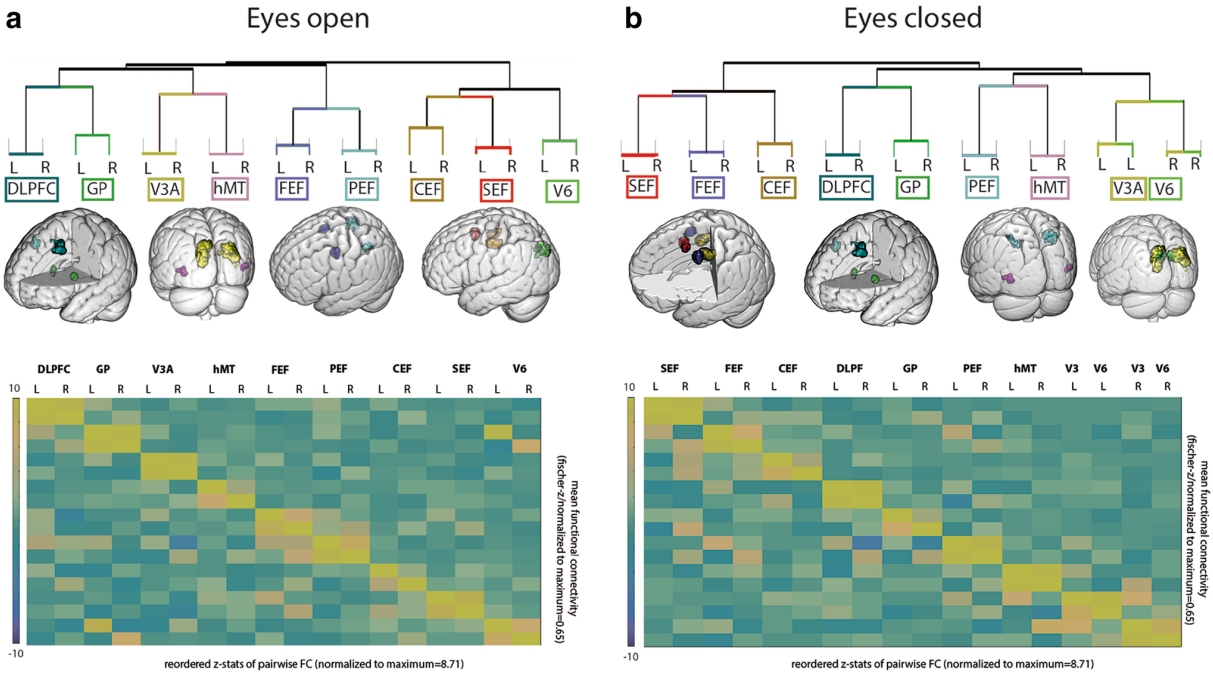

Figure 3. Hierarchical clustering of the optokinetic network in the eyes closed and eyes open resting state condition. Hierarchical clustering results are presented in a compound dendrogram. The relative height of a node indicates the distance value between the different cluster. **(a)** In the eyes open condition, hierarchical clustering analysis revealed a separate subgrouping of higher order visual and oculomotor regions (right subcluster, CEF, beige, and SEF, red, V6, green) and executive ocuolomotor (left subcluster, right subgroup, FEF, dark blue, and PEF, cyan) afferent intermediate level visual motion processing regions (middle subgroup, V3A, yellow, and hMT, violet) and subcortical modulating regions (leftmost subgroup, DLPFC, dark green, and GP, light green). The localization of the seed regions in their respective subgroup is depicted in render view below the dendrograms. The matrix below depicts the mean functional connectivity of the respective seeds, and the scale at the left of the matrix represents z scores (yellow + 10, blue − 10). **(b)** In the eyes closed condition, a subgrouping of regions which form part of the visual stream (rightmost subgroup, from right to left: V6, green; V3A, yellow; hMT, violet; PEF, light blue) and of predominantly oculomotor related regions (leftmost subgroup, SEF, red; FEF, dark blue; CEF, beige) was observed.

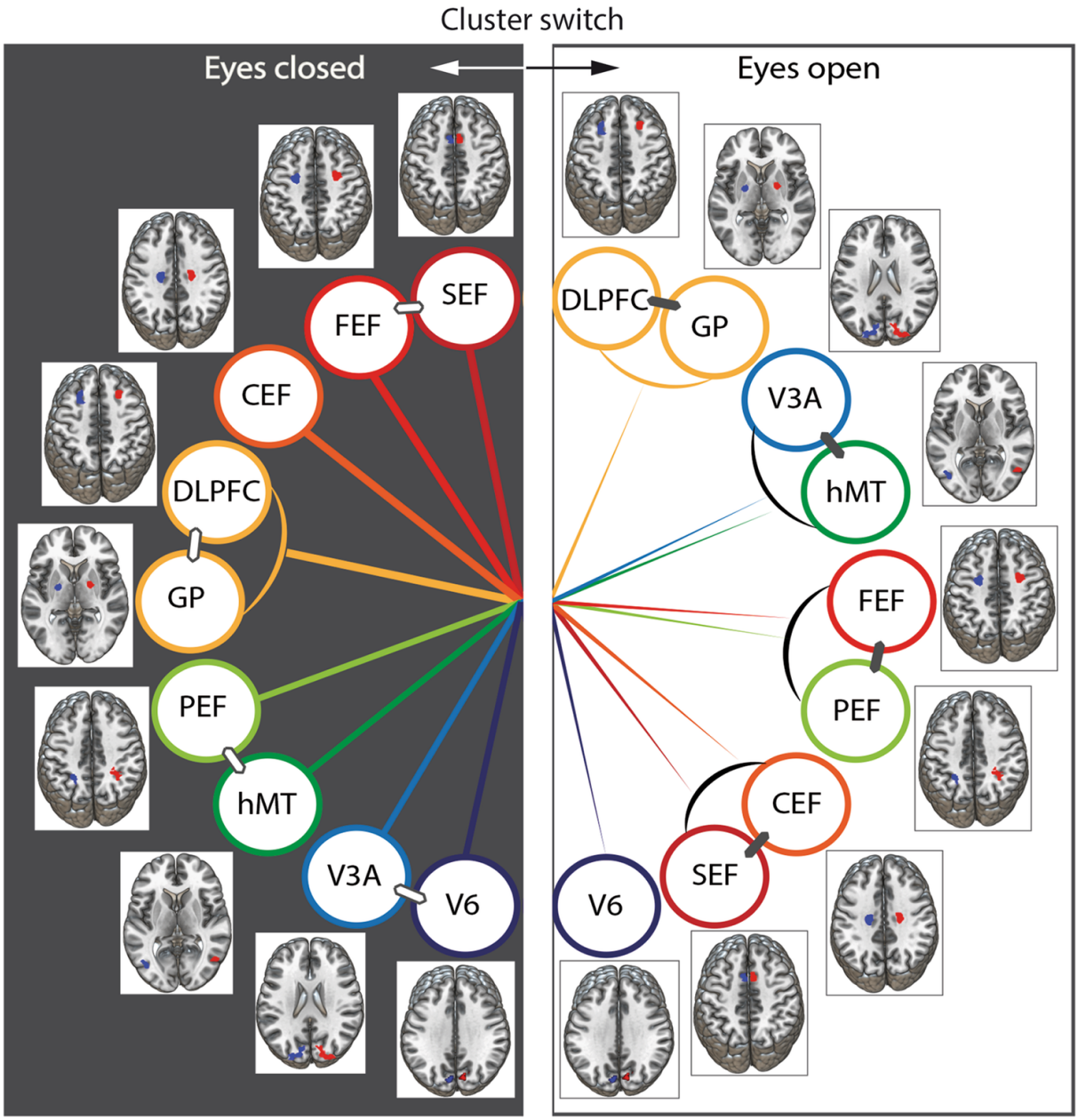

Figure 4. Schematic draft of changes in the subclustering of the optokinetic hubs in both resting state conditions. The circle depicts the switches in the subgrouping of the different optokinetic hubs schematically. Each hub is presented with a slice view of the respective seed region (region in the right hemisphere in red and region in the left hemisphere in blue). Bars between the hubs indicate that they belong to the same subcluster. The respective hubs in both conditions are connected via lines to mark the change of subclustering. In the eyes closed condition (left part of circle), SEF (dark red) and FEF (light red) build a subcluster and are grouped together with CEF (orange-red); DLPFC and GP build a separate subcluster; PEF (light green) and hMT (dark green) build a subcluster and are in the same subgroup with V3A (light blue) and V6 (dark blue). For illustrative purposes, colours of the individual hubs are maintained in the eyes open condition on the right. Here, DLPFC and GP form a constant subcluster, whereas SEF (dark red) switches the subcluster together with CEF (orange–red); FEF builds a subcluster with PEF, hMT clusters with V3A, and V6 builds a separate subcluster.

Tables

Table 1. Results of the comparisons (t-contrasts) for all OKN conditions (FDR corrected at voxel level, p<0.05, cluster threshold 10 voxel)

t-contrast	Brain area	Functional area	x y z		Cluster size		*t*value
OKN > rest							
Activations							
Cluster 1	R. calcarine gyrus		8	− 70	22	10,504	13.50
	L. cuneus	V3A	− 8	− 80	34		12.78
	L. cuneus	V3A	2	– 74	26		11.59
	R. cuneus	V3A	14	– 78	28		11.36
	L. posterior parietoocipital sulcus	V6	− 4	− 80	28		10.21
	R. posterior parietoocipital sulcus	V6	12	− 76	28		10.16
	L. superior temporal sulcus	MT/V5	− 41	76	12		10.98
	L. inferior parietal lobule	PEF	− 26	− 52	52		5.51
	R. postcentral gyrus	PEF	36	− 44	52		6.33
Cluster 2	L. putamen		− 24	2	10	1147	8.67
	L. globus pallidus		− 22	− 4	10		6.16
	L. putamen		− 14	0	14		5.08
	L. anterior insula		− 32	14	8		4.11
	R. globus pallidus		20	− 2	8		6.96
Cluster 3	R. precentral gyrus		46	− 6	50	9718	8.42
	L. precentral gyrus		− 50	− 14	57		7.69
	R. middle frontal gyrus	FEF	30	− 2	50		5.82
	L. posterior-medial frontal gyrus	SEF	− 6	4	54		5.71
	L. middle frontal gyrus	FEF	− 24	− 6	52		5.7
	R. posterior-medial frontal gyrus	SEF	8	8	42		4.82
Cluster 4	R. thalamus (parietal)		20	– 24	6	203	6.47
	R. thalamus		16	– 22	14		5.83
Cluster 5	L. posterior midcingulate cortex	CEF	− 10	− 18	44	133	6.16
Cluster 6	L. thalamus		− 22	− 28	4	68	5.43
	L. thalamus		− 20	− 28	12		4.41
Cluster 7	R. inferior temporal gyrus	Area PFcm	60	− 34	22	119	4.26
Cluster 8	R. middle frontal gyrus		50	50	6	59	4.14
	R. posterior midcingulate cortex		14	– 24	46	65	3.84
Cluster 9	L. thalamus		− 4	− 18	18	26	3.62
Cluster 10	R. middle frontal gyrus		32	48	36	88	3.30
Cluster 11	L. inferior parietal lobule	Area PFcm	− 50	− 44	25	19	3.25
Deactivations							
Cluster 1	R. rolandic operculum	Area OP3	44	− 14	20	1525	7.83
	R. posterior insula	Area Ig2	40	− 18	14		6.55
	R. parietal operculum	Area OP3	36	− 6	14		6.20
	L. rolandic operculum	Area OP3	− 44	− 14	16	1262	7.42
	L. posterior insula	Area Ig2	− 38	− 22	19		7.13
Cluster 2	R. angular gyrus	PGp	42	– 74	38	1096	6.58

	R. angular gyrus		36	– 70	50		5.86
	R. angular gyrus	PGa	46	– 60	54		5.62
Cluster 3	L. midcingulate cortex		− 8	− 38	42	3141	6.04
	R. postcentral gyrus		50	− 24	62		6.02
	L. precentral gyrus		− 32	− 26	56		5.38
	R. precentral gyrus		30	− 28	61		5.23
Cluster 4	L. superior medial gyrus		0	38	54	1626	5.96
	L. middle frontal gyrus	DLPFC	− 24	22	50		5.22
	L. superior frontal gyrus		− 20	14	56		5.05
Cluster 5	R. middle frontal gyrus	DLPFC	26	22	40	591	5.89
Cluster 6	L. anterior cingulate cortex		− 4	26	24	1408	5.38
	L. anterior cingulate cortex		− 4	34	22		5.36
Cluster 7	L. thalamus		0	– 20	6	102	5.29
Cluster 8	L. hippocampus		− 18	− 38	6	34	5.23
Cluster 9	L. inferior frontal gyrus		− 34	18	26	55	4.45
Cluster 10	L. superior parietal lobule		− 32	− 72	54	752	4.39
	L. inferior parietal lobule	Area PGa	− 50	− 66	44		4.37
	L. middle occipital gyrus	Area PGp	− 44	− 78	34		4.08
Cluster 11	R. superior frontal gyrus	Area Fp1	22	64	10	142	3.86
Cluster 12	R. thalamus		10	− 28	8	18	3.56
Cluster 12	R. posterior cingulate cortex		6	− 42	16	31	3.50
OKN stimulation right > left							
Cluster 1	R. middle occipital gyrus		34	− 78	22	2085	8.90
	R. precuneus		14	– 68	56		6.57
	R. calcarine gyrus	V3A	20	− 78	50		5.95
	R. precuneus	Area 7P	14	− 68	56		6.57
	R. intraparietal sulcus	PEF	26	− 50	52		3.44
Cluster 2	L. calcarine gyrus	Area hOc2 (V2)	−10	− 74	16	23	4.25
OKN stimulation left > right							
Cluster 1	L. middle occipital gyrus	PEF	− 30	− 80	20	2315	7.11
	L. middle occipital gyrus	PEF	− 24	− 78	26		6.63
	L. superior parietal lobule		− 14	− 74	54		6.14
	L. middle occipital gyrus		− 24	− 58	44		4.71
Cluster 2	L. precuneus	Area 5M (SPL)	− 6	− 50	50	31	4.59
	L. cuneus	V3A	− 24	− 86	24		4.44
OKN stimulation right > rest							
Activations							
Cluster 1	R. calcarine gyrus	Area V2	6	– 70	22	9090	13.59
	R. cuneus		14	– 78	34		13.32
	R. superior occipital gyrus		20	– 84	28		12.94
	R. cuneus	Area V3d	8	– 82	30		11.98
	L. lingual gyrus	V1	0	– 74	14		11.22
	R. postcentral gyrus	PEF	36	– 42	52		5.44
	L. posterior parietooccipital sulcus	V6	− 4	− 80	28		11.4
	R. posterior parietooccipital sulcus	V6	12	– 76	28		9.79
	L. cuneus	V3A	− 8	− 80	32		12.24

	R. cuneus	V3A	20	– 84	28		12.04
Cluster 2	R. precentral gyrus		44	− 4	52	9887	8.81
	R. precentral gyrus		50	− 2	46		8.42
	L. precentral gyrus		− 42	− 10	52		8.19
	R. middle frontal gyrus	FEF	36	− 2	58		7.47
	L. middle frontal gyrus	FEF	− 24	− 6	52		6.12
	L. posterior− medial frontal gyrus	SEF	− 6	0	60		7.08
	R. posterior− medial frontal gyrus	SEF	8	4	58		5.88
	L. inferior parietal lobule	PEF	− 26	− 52	52		4.55
	R. globus pallidus		22	0	6		4.33
Cluster 3	L posterior midcingulate cortex	CEF	− 10	− 18	44	124	6.88
Cluster 4	L inferior parietal lobule		− 26	− 56	58	1052	5.92
	L postcentral gyrus		− 34	− 36	46		4.17
Cluster 5	L putamen		− 24	4	10	760	5.84
	L insula lobe		− 30	16	8		4.70
	L globus pallidus		− 20	− 2	4		3.64
Cluster 6	R thalamus		20	– 26	6	79	3.95
	R thalamus		16	– 22	14		3.17
Cluster 7	R posterior midcingulate cortex	CEF	14	– 38	50	80	3.73
Cluster 8	L thalamus		− 22	− 28	4	12	3.32
Cluster 9	L superior temporal gyrus		− 48	− 40	20		3.16
Cluster 10	R middle frontal gyrus		36	50	30	37	2.96
Cluster 11	R superior temporal gyrus		56	− 40	18	86	2.89
	R superior temporal gyrus	Area PFcm	62	− 32	26		2.60
Deactivations							
Cluster 1	L rolandic operculum	OP3	− 40	− 16	16	766	6.61
	L rolandic operculum	OP4	− 46	− 12	12		6.19
	L superior temporal gyrus		− 52	− 18	4		5.26
	L posterior insula	Area Ig2	− 40	20	6		5.03
Cluster 2	R middle occipital gyrus	Area PGp	42	– 74	38	707	6.46
	R inferior parietal lobule	Area PGa	46	– 60	54		5.10
	R angular gyrus		36	– 70	52		4.66
Cluster 3	R rolandic operculum	OP3	42	− 12	20	1045	6.08
	R posterior insula	Area Ig2	38	− 22	14		5.32
	R rolandic operculum	OP4	46	− 10	8		5.32
Cluster 4	R precentral gyrus		38	− 20	70	973	5.50
	L precentral gyrus		− 32	− 24	58		4.56
Cluster 5	L middle frontal gyrus	DLPFC	− 24	12	48	275	5.57
	L middle frontal gyrus	DLPFC	− 24	22	50		5.22
Cluster 6	L superior medial gyrus		0	38	54	168	5.16
	L posterior− medial frontal gyrus		− 4	20	62		3.88
Cluster 7	L posterior midcingulate cortex		− 2	− 32	44	341	4.62
Cluster 8	L anterior cingulate cortex		− 4	26	24	57	4.50
Cluster 9	R middle frontal gyrus	DLPFC	26	22	40	58	4.78
	R middle frontal gyrus		26	20	42		4.26

Cluster 11	L inferior parietal lobule		− 30	− 74	52	39	3.94
Cluster 12	L middle occipital gyrus	Area PGp	− 44	− 78	34	116	3.88
Cluster 13	L posterior midcingulate cortex		− 4	− 8	44	24	3.74
Cluster 14	L superior frontal gyrus		− 24	36	50	58	3.60
Cluster 15	L superior medial gyrus	Area Fp2	− 6	52	18	28	3.36
Stimulation left > rest							
Activations							
Cluster 1	R calcarine gyrus	V2, V1	6	– 68	20	10,191	13.55
	L superior occipital gyrus		− 20	− 80	30		12.76
	L cuneus	V3A	− 12	− 84	36		12.61
	L inferior parietal lobule		− 26	− 56	60		9.62
	R postcentral gyrus	PEF	34	– 44	52		5.88
	L superior parietal lobule	PEF	− 28	− 50	56		6.27
	R posterior parietooccipital sulcus	V6	12	– 76	28		9.67
	L posterior parietooccipital sulcus	V6	− 6	− 82	26		8.4
	L cuneus	V3A	14	– 78	28		8.59
Cluster 2	L precentral gyrus		− 42	− 10	52	8164	8.32
	R precentral gyrus		46	− 4	50		8.29
	L superior frontal gyrus	FEF	− 24	− 6	52		7.38
	R superior frontal gyrus	FEF	28	− 4	52		5.66
	L posterior− medial frontal gyrus	SEF	− 4	4	54		6.05
	R posterior− medial frontal gyrus	SEF	8	4	54		4.26
Cluster 3	L putamen		− 24	2	12	722	6.53
	L insula lobe		− 32	16	8		3.88
	L globus pallidus		− 24	− 6	6		7.19
Cluster 4	R putamen		24	0	10	405	4.77
	R globus pallidus		22	− 2	8		7.14
Cluster 5	L posterior midcingulate cortex	CEF	− 10	− 18	44	113	6.09
Cluster 6	R middle temporal gyrus		42	– 62	14	51	5.35
Cluster 7	R middle frontal gyrus		48	48	6	43	3.88
Cluster 8	R middle frontal gyrus		38	42	38	175	3.53
Cluster 9	L postcentral gyrus	Area 3b	− 56	− 20	36	71	3.49
Cluster 10	R postcentral gyrus	Area 3b	56	− 14	34	29	2.99
Cluster 11	R superior temporal gyrus	Area PFcm	60	− 32	20	33	2.89
Cluster 12	R posterior midcingulate cortex	CEF	14	– 22	46	16	2.71
Deactivations							
Cluster 1	L rolandic operculum	OP3	− 40	− 16	16	1048	7.04
	L rolandic operculum	OP4	− 46	− 12	12		6.61
	L posterior insula	Area Ig2	− 38	− 20	6		6.05
Cluster 2	R rolandic operculum	OP3	40	− 14	20	1271	6.08
	R rolandic operculum	OP3	40	− 10	6		6.03
	R superior temporal gyrus		56	− 16	8		5.21
Cluster 3	R middle occipital gyrus	Area PGp	42	– 74	38	897	5.56
	R inferior parietal lobule	Area PGa	48	– 60	52		5.48

	R angular gyrus	Area PGp	36	– 70	52		5.24
Cluster 4	L posterior midcingulate cortex		− 2	− 8	44	129	5.53
	R anterior cingulate cortex		2	4	34		3.16
Cluster 5	R middle frontal gyrus	DLPFC	26	24	42	346	5.79
	R middle frontal gyrus	DLPFC	26	22	40		5.49
Cluster 6	L precentral gyrus		− 30	− 26	60	401	5.40
Cluster 7	L superior medial gyrus		− 2	38	54	1696	5.02
	L middle frontal gyrus	DLPFC	− 28	18	58		5.1
	L middle frontal gyrus		− 26	18	56		4.91
Cluster 8	R precentral gyrus		36	− 24	70	945	4.76
	R postcentral gyrus	Area 4a	18	– 38	76		4.29
Cluster 9	L angular gyrus	Area PGp	− 48	− 68	46	555	4.64
	L inferior parietal lobule	Area 7A	− 32	− 74	52		4.62
Cluster 10	L posterior midcingulate cortex		0	– 36	40	442	4.54
Cluster 11	Left thalamus		0	– 20	6	18	3.59
	Left thalamus		− 16	− 36	6	15	3.38
Cluster 12	L superior frontal gyrus	Area Fp1	− 18	60	22	51	3.21
	L superior medial gyrus	Area Fp2	0	58	8	42	3.18
	R middle orbital gyrus	Area Fp2	4	48	0	36	3.15
	L middle temporal gyrus		− 38	− 54	26	21	3.03